limited primarily by elastic scattering from the potential disorder. Given that the oxygen dopants responsible for this potential disorder do not reside in the CuO_2 plane, scattering is relatively weak. This can result in a longer mean free path and the measured 100 Å length scale is therefore quite reasonable. As scattering into all angles is involved in ARPES measurements, whereas transport is dominated by large-angle scattering of the nodal quasiparticles, our results may also reconcile the discrepancy between the mean free path measured by transport[15] as compared to that measured by ARPES. Taking 14 Å as the length scale over which the disorder potential varies significantly, we deduce that the dominant elastic scattering process is limited by the wavevector $q = 1/14\,\text{Å}^{-1}$. The scattering angle, θ, given by $\sin(\theta/2) = q/2k_F$, where k_F is the Fermi wavevector, is indeed quite small at about $5°$, which provides a possible explanation as to why the transport mean free path can be much longer than that measured by ARPES.

Discussion of our observations can also be extended to more fundamental issues, such as the coherence of the superconducting state. The coexistence of a high superconducting transition temperature with such a microscopic inhomogeneity implies that the superconducting coherence length is shorter than the mean free path. Our measured gap correlation length, $\xi \approx 14$ Å, sets the length scale for the superconducting pair size in optimally doped $Bi_2Sr_2CaCu_2O_{8+x}$. By evaluating the BCS expression $\xi_0 = \hbar v_F/\pi\Delta$, taking $\hbar v_F = 1.6\,\text{eVÅ}$ from band dispersion near the nodes[14,16] and the averaged gap at optimal doping as $\Delta = 0.04\,\text{eV}$, we obtain $\xi_0 \approx 13$ Å, which is in good agreement with the correlation decay length ξ obtained from our experiment. Yet ξ appears to be shorter than the experimental in-plane superconducting coherence length $\xi_{ab} \approx 22–27$ Å (refs 17–19). In contrast to conventional BCS superconductors, it is conceivable that the amplitude and phase coherence in high-T_c superconductors have different length scales, because the ratio $R = 2\Delta/k_BT_c$, is no longer a constant. Recent ARPES measurements[11] suggest that $R \propto 1/x$. Thus we may expect the superconducting phase coherence length to be determined by $\hbar v_F/k_BT_c$, which scales as $1/x$ on the underdoped side. An extension of our correlation length and vortex core-size measurements to underdoped samples with various doping concentrations will perhaps distinguish the two length scales because they may have different doping (x) dependences.

The observation of microscopic spatial variations in both the carrier density and the superconducting gap, and the strong correlation between these variations, reveals the local inhomogeneous charge environment in these materials, and its intimate relationship with superconductivity. Further exploration of this frontier may lead to a greater understanding of how high-T_c superconductivity arises from doping a Mott insulator. □

1. Anderson, P. W. *The Theory of Superconductivity in the High-T_c Cuprates* (Princeton Univ. Press, Princeton, New Jersey, 1997).
2. Hudson, E. W., Pan, S. H., Gupta, A. K., Ng, K.-W. & Davis, J. C. Atomic-scale quasiparticle scattering resonances in Bi₂Sr₂CaCu₂O₈₊δ. *Science* **285**, 88–91 (1999).
3. Pan, S. H. *et al.* Imaging the effects of individual zinc impurity atoms on superconductivity in Bi₂Sr₂CaCu₂O₈₊δ. *Nature* **403**, 746–750 (2000).
4. Renner, Ch. *et al.* Pseudogap precursor of the superconducting gap in under- and overdoped Bi₂Sr₂CaCu₂O₈₊δ. *Phys. Rev. Lett.* **80**, 149–152 (1998).
5. Miyakawa, N. *et al.* Predominantly superconducting origin of large energy gaps in underdoped Bi₂Sr₂CaCu₂O₈₊x from tunneling spectroscopy. *Phys. Rev. Lett.* **83**, 1018–1021 (1999).
6. Hasegawa, H., Ikuta, H. & Kitazawa, K. in *Physical Properties of High Temperature Superconductors III* (ed. Ginsberg, D. M.) Ch. 7 (World Scientific, Singapore, 1992).
7. Wolf, E. L., Chang, A., Rong, Z. Y., Ivanchenko, Yu. M. & Lu, F. Direct STM mapping of the superconducting energy gap in single crystal Bi₂Sr₂CaCu₂O₈₊x. *J. Superconductivity* **70**, 355–360 (1994).
8. Ino, A. *et al.* Doping dependent density of states and pseudogap behavior in La₂₋ₓSrₓCuO₄. *Phys. Rev. Lett.* **81**, 2124–2127 (1998).
9. Fong, H. F. *et al.* Neutron scattering from magnetic excitations in Bi₂Sr₂CaCu₂O₈₊δ. *Nature* **398**, 588–591 (1999).
10. Feng, D. L. *et al.* Signature of superfluid density in the single-particle excitation spectrum of Bi₂Sr₂CaCu₂O₈₊δ. *Science* **289**, 277–281 (2000).
11. Ding, H. *et al.* Coherent quasiparticle weight and its connection to high-T_c superconductivity from angle-resolved photoemission. Preprint cond-mat/0006143 at ⟨http://xxx.lanl.gov⟩ (2000).
12. Valla, T. *et al.* Temperature dependent scattering rates at the Fermi surface of optimally doped Bi₂Sr₂CaCu₂O₈₊δ. *Phys. Rev. Lett.* **85**, 828–831 (2000).
13. Valla, T. *et al.* Evidence for quantum critical behavior in the optimally doped cuprate Bi₂Sr₂Ca-Cu₂O₈₊δ. *Science* **285**, 2110–2113 (1999).
14. Kaminski, A. *et al.* Quasiparticles in the superconducting state of Bi₂Sr₂CaCu₂O₈₊δ. *Phys. Rev. Lett.* **84**, 1788–1791 (2000).
15. Zhang, Y. *et al.* Giant enhancement of the thermal Hall conductivity κ_xy in the superconductor YBa₂Cu₃O₇. Preprint cond-mat/0008140 at ⟨http://xxx.lanl.gov⟩ (2000).
16. Bogdanov, P. V. *et al.* Evidence for an energy scale for quasiparticle dispersion in Bi₂Sr₂CaCu₂O₈₊δ. *Phys. Rev. Lett.* **85**, 2581–2584 (2000).
17. Palstra, T. T. M. *et al.* Angular dependence of the upper critical field of Bi₂Sr₂CaCu₂O₈₊δ. *Phys. Rev. B* **38**, 5102–5105 (1988).
18. Renner, Ch., Revaz, B., Kadowaki, K., Maggio-Aprile, I. & Fischer, Ø. Observation of the low temperature pseudogap in the vortex cores of Bi₂Sr₂CaCu₂O₈₊δ. *Phys. Rev. Lett.* **80**, 3606–3609 (1998).
19. Pan, S. H. *et al.* STM studies of the electronic structure of vortex cores in Bi₂Sr₂CaCu₂O₈₊δ. *Phys. Rev. Lett.* **85**, 1536–1539 (2000).

....

Friction and fracture

Eric Gerde & M. Marder

Computational and Applied Mathematics and Center for Nonlinear Dynamics, The University of Texas at Austin, Austin, Texas 78712, USA

....

Consider a block placed on a table and pushed sideways until it begins to slide. Amontons and Coulomb found that the force required to initiate sliding is proportional to the weight of the block (the constant of proportionality being the static coefficient of friction), but independent of the area of contact[1]. This is commonly explained by asserting that, owing to the presence of asperities on the two surfaces, the actual area in physical contact is much smaller than it seems, and grows in proportion to the applied compressive force[1]. Here we present an alternative picture of the static friction coefficient, which starts with an atomic description of surfaces in contact and then employs a multiscale analysis technique to describe how sliding occurs for large objects. We demonstrate the existence of self-healing cracks[2–4] that have been postulated to solve geophysical paradoxes about heat generated by earthquakes[5–11,25–27], and we show that, when such cracks are present at the atomic scale, they result in solids that slip in accord with Coulomb's law of friction. We expect that this mechanism for friction will be found to operate at many length scales, and that our approach for connecting atomic and continuum descriptions will enable more realistic first-principles calculations of friction coefficients.

The most intriguing fact about friction is that it is proportional to the force pushing two objects together, but independent of the area of contact. Without contesting the prevalence of materials where the conventional picture involving asperities applies, we wish to point out an alternative way of explaining the same basic fact. Suppose two solids are in close contact over some distance. Suppose further that a wave of separation, a self-healing crack, can run along the interface, like a bump on a rug, leading one solid to slip over the other (Fig. 1). And suppose finally that the condition for such self-

healing cracks to arise depends only upon the ratio of horizontal to compressive stress. Then sliding begins in accord with Coulomb's law, and is naturally independent of the area of contact.

We can demonstrate in a simple but realistic setting that these suppositions are correct. We begin by describing a calculation that employs standard techniques from continuum mechanics[12–14]. Imagine a semi-infinite elastic solid atop a rigid substrate, impose vertical and horizontal stresses σ_{yy} and σ_{xx} far from the boundary, and suppose that there is a self-healing crack of length l, travelling at speed v, and causing slip of amount Δu (Fig. 1). For all values of these five parameters we can calculate stress and displacement fields everywhere in the elastic solid, including cases where σ_{yy} is compressive[13,14]. However, there is a problem—all of these solutions have an unphysical feature. Sufficiently near each crack tip, the crack faces oscillate and pass through each other infinitely often. Perhaps none of the solutions can actually occur in a physical system. On the other hand, if the intersections occur on a scale much smaller than an interatomic spacing, is there really a problem? The possibility of solids sliding over one another as we describe hinges upon the existence of self-healing cracks. Finding explicit solutions in continuous media has not been hard, but it has been difficult to establish a consensus on whether or not the solutions are physically acceptable[15,16]. The physical problem has been recast in a number of mathematical contexts. For example, one can investigate two surfaces that remain absolutely flat and in contact at all times, with a friction law allowing them to move relative to one another[14,15]. However, so long as the problem is stated in the continuum, the essential difficulty persists.

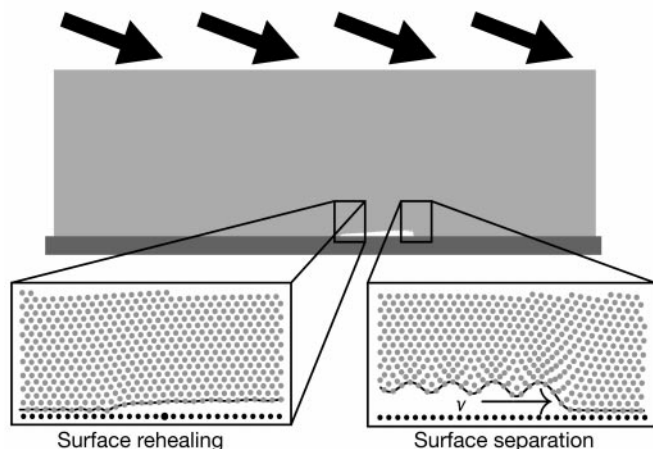A way to resolve the conceptual problems is to leave continuum

Figure 1 Numerical simulation of a self-healing crack travelling through a compressed strip. The block slips by a distance of three atoms over the lower surface when the self-healing crack moves from left to right. Atoms initially on a 400 by 1,200 triangular grid interact linearly with nearest neighbours. Interactions with the rigid substrate are governed by truncated hookean potentials with a bond rupture strain of 5%. Atoms from the upper block interact with any atom in the substrate that comes within range; this allows the upper surface to slip with respect to the lower and then heal. We impose fixed horizontal and vertical displacements on the top layer, and initiate dynamics with an artificially created crack. Creation of the moving crack proceeds in stages. At first, the upper layer of the system is in tension, and the tail end of the crack extends to the end of the system. Slowly the outer boundary is pushed into compression, at which point the left side of the crack closes up, and becomes self-healing. At the crack moves forward, we add new atoms to the right boundary, and remove atoms from the left. The system eventually converges to the steady-state shown here, with a self-healing crack of length $l = 168$, speed $v = 0.83 c_s$, and surface slip $\Delta u = 3$. Distances are in units of interatomic spacing, and c_s is the shear wave speed of the material. Vertical displacements have been rescaled by 3 for visual clarity.

mechanics and pose the question about self-healing cracks at the atomic level. Cracks can be followed in atomic detail as they move through solids with arbitrarily large numbers of atoms[17]. We have extended the atomic-scale analytical techniques to include the case of interface fracture.

The context for our work is the following set of equations. Atomic equilibrium positions, $\mathbf{r}_{mn}$, lie on a triangular grid N atoms high with unit interatomic spacing:

$$\mathbf{r}_{mn} = \begin{bmatrix} m - n/2 \\ \sqrt{3}/2n \end{bmatrix}, \quad \begin{array}{l} -\infty < m < \infty \\ 0 \le n \le N \end{array} \quad (1)$$

Displacements from equilibrium, $\mathbf{u}_{mn}(t)$, satisfy the steady-state equation, $\mathbf{u}_{mn}(t) = \mathbf{u}_{0n}(t - m/v)$, and the top layer is rigidly displaced, $\mathbf{u}_{mN}(t) = \begin{bmatrix} D_x \\ D_y \end{bmatrix}$. The steady-state equations of motion are:

$$\ddot{\mathbf{u}}_{mn} + b\dot{\mathbf{u}}_{mn} = \sum_{m',n' \text{ where } \|\mathbf{dr}\|=1} (\mathbf{u}_{m'n'} - \mathbf{u}_{mn}) \cdot \mathbf{dr}\,\mathbf{dr}$$

$$- \mathbf{u}_{mn} \cdot \mathbf{r}_{11}\mathbf{r}_{11}\, \theta(1/2 - n)\theta(m/v - t)$$

$$- \mathbf{u}_{mn} \cdot \mathbf{r}_{01}\mathbf{r}_{01}\, \theta(1/2 - n)\theta(m/v - t + s) \quad (2)$$

Here b is a small dissipation parameter, θ is the Heaviside function, and $\mathbf{dr} = \mathbf{r}_{m'n'} - \mathbf{r}_{mn}$. The syncopation, s, designates the time difference between left and right bond ruptures for atoms along the interface. Finally, we require bonds to reach a critical strain, u_c, before rupture, and the newly created surface to remain separated thereafter. Apart from u_c, which sets an overall scale, in the limits $N \to \infty$, $b \to 0$ each microscopic fracture state is described by two parameters—its velocity v, and syncopation s. Methods for solving this problem generalize those described in ref. 18. The main new technical hurdle is that the equations reduce to a 2×2 Wiener–Hopf system. The system is approximated with Wilson's algorithm[19] applied to an equivalent factorization problem on the unit circle[20] and solved.

The advantage of the atomic-scale analytical methods is that they can treat arbitrarily large numbers of atoms, and therefore lead to a connection with continuum analysis. However, they have an important limitation. The formal techniques only operate if bonds, once broken, never heal; they only treat semi-infinite cracks, and describe the forward tip of a self-healing crack, or its closing end, but not both at once.

The final stage of our analysis is to combine information from the continuum and the atomic solutions. The latter make it possible to determine when a crack tip is physically realizable and when it is not; the former make it possible to describe the self-healing process. The connection between continuous and atomic descriptions is created in the following way. Continuum calculations[21,22] show that stress fields sufficiently close to the tip of an interface crack at the origin have an oscillating singularity where σ_{yy} takes the form:

$$\sigma_{yy}(x,0) = \text{Re}[\tilde{K}x^{-1/2+i\epsilon}]/\sqrt{2\pi} \quad (3)$$

The real constant ϵ increases with the speed v of the crack, and the constant $\tilde{K}$ has both real and imaginary parts. Note that the sign of the stress oscillates as the crack tip is approached; the possibility of converting compressive stresses far away to tensile stresses near the tip helps explain in principle why self-healing cracks are possible.

Turning to an atomic point of view, we can find exactly the same universal form for the stress field, but it now emerges far from the tip of a semi-infinite crack. That is, by adopting a continuum perspective and 'zooming-in' on a crack tip, we find the same mathematical forms that are found by adopting an atomic perspective and 'zooming-out'. However, the atomic analysis has additional information to contribute. Once v and s are specified (see equation (2)), $\tilde{K}$ is completely determined.

Thus, the atomic analysis chooses from the five-dimensional

space of continuum solutions a subspace that is physically permitted. The precise states that are permitted depend upon details of the atomic model, but the elimination of most—but not all—continuum states should be general.

We are finally in a position to carry out an exhaustive search for self-healing cracks. The search proceeds in the following way. Fix v, l, and the total surface slip Δu. Next, fix the syncopation s_f for the forward crack tip (equation (2)) and use the atomic solutions to calculate the strength of the associated oscillating stress singularity $\tilde{K}$. Inserting this value into the macroscopic solution, determine the stresses at infinity $\sigma_{xy}(\infty)$, $\sigma_{yy}(\infty)$. Next choose a syncopation s_b for the back of the crack. Again stresses at infinity are uniquely determined—but there is no reason they should be the same as the values dictated by the front. There are two parameters s_f and s_b that can be varied, leading to a finite number of cases where $\sigma_{xy}(\infty)$, $\sigma_{yy}(\infty)$ make both the front and back propagate at the prescribed speed. We typically find no solution, or one solution, on varying s_f

and s_b within the allowable range of syncopation values, roughly $|s| < 1/|v|$.

The results of this search are illustrated in Fig. 2. In Fig. 2a, we catalogue cracks moving between 50% and 80% of the shear wave speed, in velocity increments of 1%. Figure 2b focuses on the self-healing cracks that move at 80% of the shear wave speed. (We note that strains within the Earth, given by the ratio of a characteristic stress σ_{yy} to Young's modulus E, are of the order of 10^{-4}.) The lower boundary in Fig. 2a is roughly linear, and extends down to strains of the order of 10^{-5}. The complex structure of solutions for strains below 10^{-5} results from the existence of a minimum crack-propagation speed. Such minimum speeds are typical in atomic models of fracture at zero temperature[23].

In order to check whether treating the front and the back of the crack independently at the atomic level led to errors, and to check more generally the validity of our calculations, we have performed a number of full molecular-dynamics calculations in regions of
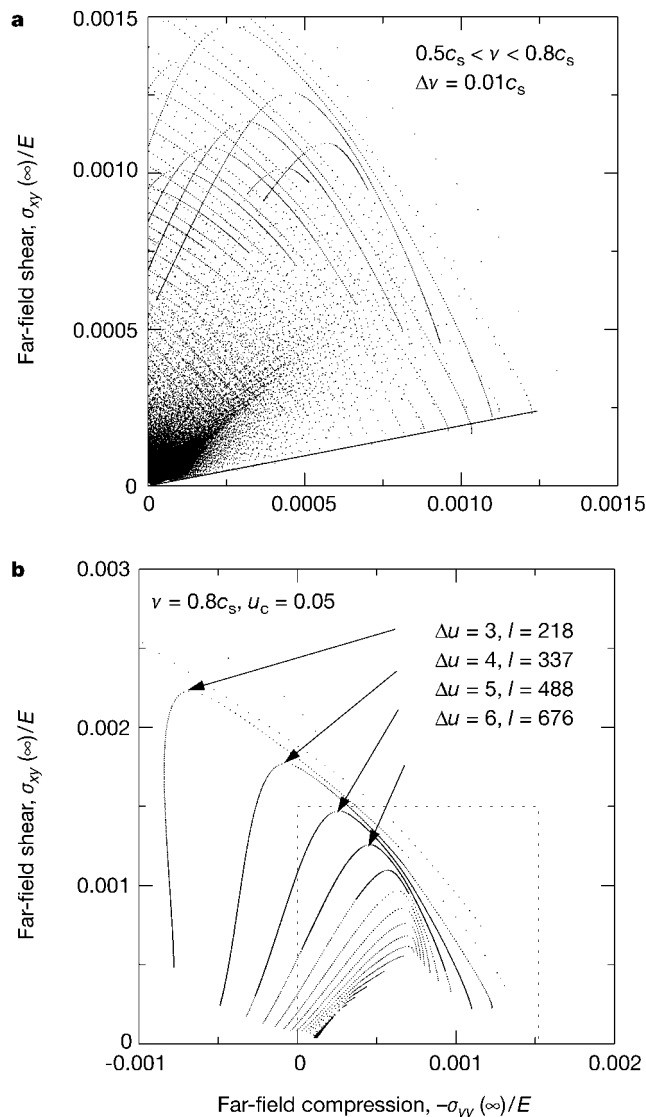

Figure 2 Catalogue of shear $\sigma_{xy}(\infty)$ and compressive $-\sigma_{yy}(\infty)$ stresses, applied to infinitely large systems, that support steadily moving self-healing cracks. **a**, Crack moving at 50–80% of the shear wave speed, in velocity increments of 1%. The minimum shear stress that allows cracks to move for a given compressive stress yields an approximately linear relationship (Coulomb's law), indicated by the straight line in **a**. The slope of this line is the friction coefficient, 0.2. Stresses are normalized by Young's modulus E and

velocities v are normalized by shear wave speed c_s. Integral values of crack length l and total slip Δu lead to a discrete set of states for each velocity v. **b**, As **a** but selecting just the self-healing cracks moving at velocity $v = 0.8c_s$. Points that appear to form a curve have the same slip Δu but different crack lengths l. The region inside the box with dotted outline is shown in **a**.

parameter space where self-healing cracks were predicted to exist. Because of the long running times and complicated initial conditions needed to produce steady states, we have limited ourselves to small systems of about 500,000 atoms. We have found three self-healing cracks consistent with the analytical predictions; a picture of one of them appears in Fig. 1.

With the catalogue of self-healing cracks in hand, we now return to the matter of how they lead to friction. For any given compressive stress $(-\sigma_{yy}(\infty))$ there is a minimum shear stress $\sigma_{xy}(\infty) \approx -0.2\sigma_{yy}(\infty)$ that allows the cracks to begin moving (see Fig. 2a). For any smaller shear stress, the upper block cannot slide; for any larger shear stress, there is a way for it to slide. This sliding is well described by a coefficient of friction to the extent that the lower boundary of states can be approximated by a straight line. The lower boundary of states depends only weakly upon the model parameters, which include bond stiffness and interface strength.

What we have in fact determined is a lower bound on a coefficient of static friction at zero temperature. Static friction will be determined by when self-healing cracks actually initiate, which is not necessarily identical with when they first become possible. Once sliding begins, properties of kinetic friction will be determined by populations of self-healing cracks. The speed at which the upper block slides will depend upon the number of self-healing cracks moving at any time, and is not directly determined by the speeds of these cracks.

The question of when self-healing cracks actually underlie frictional sliding will have to be settled by experiments. There is some evidence for such cracks from experiments aimed at settling questions about earthquakes[5–7]. Real surfaces are certainly not flat enough over macroscopic lengths for our description of friction to be complete, and other mechanisms of frictional sliding[1,24] will certainly compete with this one. However, we believe that our calculation of a friction coefficient from the atomic scale up constitutes progress. We hope that these definite mathematical results for an ideal case will be useful for proceeding to more realistic ones, and will motivate new experiments. □

1. Persson, B. N. J. *Sliding Friction: Physical Principles and Applications* (Springer, Heidelberg, 1998).
2. Comninou, M. & Dundurs, J. Can solids slide without slipping? *Int. J. Solids Struct.* **14,** 251–260 (1978).
3. Weertman, J. Unstable slippage across a fault that separates elastic media of different elastic constants. *J. Geophys. Res. B* **85,** 1455–1461 (1980).
4. Caroli, C. Slip pulses at a sheared frictional viscoelastic/nondeformable interface. *Phys. Rev. E* **62,** 1729–1735 (2000).
5. Brune, J. N., Brown, S. & Johnson, P. A. Rupture mechanism and interface separation in foam rubber models of earthquakes: a possible solution to the heat flow paradox and the paradox of large overthrust. *Tectonophysics* **218,** 59–67 (1993).
6. Brown, S. R. Frictional heating on faults: Stable sliding versus stick slip. *J. Geophys. Res.* **103,** 7413–7420 (1998).
7. Anooshehpoor, A. & Brune, J. N. Wrinkle-like Weertman pulse at the interface between two blocks of foam rubber with different velocities. *Geophys. Res. Lett.* **26,** 2025–2028 (1999).
8. Scott, R. S. Seismicity and stress rotation in a granular model of the brittle crust. *Nature* **381,** 5922–595 (1996).
9. Ben-Zion, Y. & Andrews, D. J. Properties and implications of dynamic rupture along a material interface. *Bull. Seismol. Soc. Am.* **88,** 1085–1094 (1998).
10. Mora, P. The weakness of earthquake faults. *Geophys. Res. Lett.* **26,** 123–126 (1999).
11. Place, D. & Mora, P. The lattice solid model to simulate the physics of rocks and earthquakes: incorporation of friction. *J. Comput. Phys.* **150,** 332–372 (1999).
12. Freund, L. B. *Dynamic Fracture Mechanics* (Cambridge Univ. Press, Cambridge, 1990).
13. Dhaliwal, R. J. & Saxena, H. S. Moving Griffith crack at the interface of two orthotropic elastic layers. *J. Math. Phys. Sci.* **26,** 237–254 (1992).
14. Das, S. & Patra, B. Moving Griffith crack at the interface of two dissimilar orthotropic half planes. *Eng. Fract. Mech.* **54,** 523–531 (1996).
15. Ranjith, K. & Rice, J. R. Slip dynamics at an interface between dissimilar materials. *J. Mech. Phys. Solids* **49,** 341–361 (2001).
16. Cochard, A. & Rice, J. R. Fault rupture between dissimilar materials: III-posedness, regularization, and slip-pulse response. *J. Geophys. Res. B* **105,** 25891–25907 (2001).
17. Slepyan, L. I. Plane problem of a crack in a lattice. *Izv. Akad. Nauk SSSR Mekh. Tverd. Tela* **16,** 101–115 (1982).
18. Marder, M. & Gross, S. Origin of crack tip instabilities. *J. Mech. Phys. Solids* **43,** 1–48 (1995).
19. Wilson, G. T. The factorization of matrixial spectral densities. *SIAM J. Appl. Math.* **23,** 420–426 (1972).
20. Eggermont, P. & Lubich, C. Fast numerical solution of singular integral equations. *J. Integral Equations Appl.* **6,** 335–351 (1994).
21. Williams, M. L. The stresses around a fault or crack in dissimilar media. *Bull. Seismol. Soc. Am.* **49,** 199–204 (1959).
22. Deng, X. Complete complex series expansions of near-tip fields for steadily growing interface cracks in dissimilar isotropic materials. *Eng. Fract. Mech.* **42,** 237–242 (1992).
23. Holland, D. & Marder, M. Cracks and atoms. *Adv. Mater.* **11,** 793–806 (1999).
24. Müser, M. H., Wenning, L. & Robbins, M. O. Simple microscopic theory of Amontons's laws for static friction. *Phys. Rev. Lett.* **86,** 1295–1298 (2001).
25. Heaton, T. H. Evidence for and implications of self-healing pulses of slip in earthquake rupture. *Phys. Earth Planet. Interiors* **64,** 1–20 (1990).
26. Adams, G. G. Dyanmic motion of two elastic half-spaces in relative sliding without slipping. *J. Tribol.* **121,** 455–461 (1999).
27. Ranjith, K. & Rice, J. R. Slip dynamics at an interface between dissimilar materials. *J. Mech. Phys. Solids* **49,** 341–361 (2001).

....

A high-strain-rate superplastic ceramic

B.-N. Kim, K. Hiraga, K. Morita & Y. Sakka

National Institute for Materials Science, 1-2-1 Sengen, Tsukuba, Ibaraki 305-0047, Japan

....

High-strain-rate superplasticity describes the ability of a material to sustain large plastic deformation in tension at high strain rates of the order of 10^{-2} to $10^{-1}\,s^{-1}$ and is of great technological interest for the shape-forming of engineering materials. High-strain-rate superplasticity has been observed in aluminium-based[1] and magnesium-based[2] alloys. But for ceramic materials, superplastic deformation has been restricted to low strain rates of the order of 10^{-5} to $10^{-4}\,s^{-1}$ for most oxides[3,4] and nitrides[5] with the presence of intergranular cavities leading to premature failure. Here we show that a composite ceramic material consisting of tetragonal zirconium oxide, magnesium aluminate spinel and α-alumina phases exhibits superplasticity at strain rates up to $1\,s^{-1}$. The composite also exhibits a large tensile elongation, exceeding 1,050 per cent for a strain rate of $0.4\,s^{-1}$. The tensile flow behaviour and deformed microstructure of the material indicate that superplasticity is due to a combination of limited grain growth in the constitutive phases and the intervention of dislocation-induced plasticity in the zirconium oxide phase. We suggest that the present results hold promise for the application of shape-forming technologies to ceramic materials.

In superplastic materials, the primary deformation mechanism is grain-boundary sliding, and it is the rate of this process that determines the macroscopic strain rate. Because cavitation due to grain-boundary sliding must be accommodated by diffusion and/or dislocation processes for successive deformation, a short accommodation length—which means a small grain size—is indispensable for attaining high-strain-rate superplasticity. For the same reason, stability of the small grain size is also essential. If grain growth occurs actively during deformation, the accommodation length increases and retards facile grain-boundary sliding. This causes an increase in the level of stress necessary for successive deformation—that is, strain-hardening. Strain-hardening enhances the extent of stress concentration on the sliding grain boundaries or grain corners, resulting in the formation of intergranular cavities that leads to premature failure. We have fabricated a multi-phase